Hydrol. Earth Syst. Sci. Discuss., 12, 12167–12214, 2015
www.hydrol-earth-syst-sci-discuss.net/12/12167/2015/
doi:10.5194/hessd-12-12167-2015

Hydrology and Earth System Sciences
Open Access
Discussions

Identification of the main attribute of river flow temporal variations in the Nile Basin

C. Onyutha[1,2] **and P. Willems**[1,3]

[1]Hydraulics Laboratory, KU Leuven, Kasteelpark Arenberg 40, 3001 Heverlee, Belgium
[2]Faculty of Technoscience, Muni University, P.O. Box 725, Arua, Uganda
[3]Department of Hydrology and Hydraulic Engineering, Vrije Universiteit Brussel, Pleinlaan 2, 1050 Elsene, Brussel, Belgium

Received: 2 November 2015 – Accepted: 9 November 2015 – Published: 20 November 2015

Correspondence to: C. Onyutha (conyutha@gmail.com)

Published by Copernicus Publications on behalf of the European Geosciences Union.

Abstract

Temporal variation of monthly flows was investigated at 18 Discharge Measurement Stations (DMS) within the Nile Basin in Africa. The DMS were grouped using a clustering procedure based on the similarity in the flow variation patterns. The co-variation of the rainfall and flow was assessed in each group. To investigate the possible change in catchment behavior, which may interfere with the flow–rainfall relationship, three rainfall–runoff models were applied to the major catchment in each group based on the data time period falling within 1940–2003. The co-occurrence of the changes in the observed and simulated overland flow was examined using the cumulative rank difference (CRD) technique and the quantile perturbation method (QPM). Two groups of the DMS were obtained. Group 1 comprises the DMS from the equatorial region and/or South Sudan, while those in Sudan, Ethiopia and Egypt form group 2. In the selected catchment of each group, the patterns of changes in terms of the CRD sub-trends and QPM anomalies for both the observed and simulated flows were in a close agreement. These results indicate that change in catchment behavior due to anthropogenic influence in the Nile basin over the selected time period was minimal. Thus, the overall rainfall–runoff generation processes of the catchments were not impacted upon in a significant way. The temporal flow variations could be attributed mainly to the rainfall variations.

1 Introduction

Some of the formidable challenges that the Nile Basin faces include: floods and droughts due to climate variability, restive trans-boundary management issues, widespread poverty, high demographic growth rates, food insecurity resulting from a combined effect of rainfall variability and the unswerving dependence of majority of the population on subsistence and rain-fed agriculture, etc. To deal with these challenges, sufficient planning and management of the River Nile water resources is re-

quired. One form of support to such requirement is the enhanced comprehension of the historical patterns of flow variation and their spatial differences across the entire Nile Basin as done in this study. So far several investigations were made on the variability of flow and hydro-climatic variables for the Nile Basin (see among others Abtew et al., 2009; Camberlin, 1997; Tierney et al., 2013). Such studies give the evidence that the variability in hydro-climatic variables such as rainfall over the study area can be explained by the variations in large-scale ocean–atmosphere interactions. On the other hand, land-use changes in the different parts of the Nile Basin have been reported e.g. by Mango et al. (2011), and Olang and Fürst (2011) for the equatorial region; Bewket and Sterk (2005), Legesse et al. (2003, 2004), Rientjes et al. (2011) for Ethiopia; and Elmqvist (2005) for Sudan. Land-use changes may be ascribed to anthropogenic influence on the catchment system.

In a detailed way, the effect of the change in catchment characteristics on the watershed hydrology can be investigated using fully distributed process-based hydrological models and an archive of aerial photos or satellite images of land cover with high spatial and temporal resolutions for long time periods. However, such land use information of the specified quality and data length is difficult to obtain. Moreover, the input data required by the fully distributed process-based hydrological models are of large amount. Besides, due to their structural complexity and over-parameterization, the parameters of such models are difficult to optimally estimate. Alternatively, conceptual models that are more parsimonious hence with fewer parameters than the physically-based models can be applied to assess changes in catchment response in a meteorological-river flow data based way and at a lumped catchment scale as applied in this study.

More specifically, this study aimed at: (1) analyzing the spatiotemporal variation in annual and seasonal flows along the main rivers of the Nile Basin, (2) investigating the co-variation of flow and rainfall, and (3) rainfall–runoff modeling to investigate the evidence of changes in rainfall-flow catchment response behavior. The modeling is done at daily time scale in order to explain aggregated variations at larger temporal scale.

2 Study area and data

2.1 Study area

As one of the longest rivers in the world, River Nile that traverses 11 countries of Africa goes through a restively long journey of 6695 km from its furthest source (Ruvyironza in Kagera Basin) to the Nile Delta in Egypt. The drainage area of the River Nile with the coverage from 31° N to 4° S (in north–south direction) and 24 to 40° E (in west–east direction) is about 3 400 000 km^2 (Fig. 1). The lakes within the River Nile Basin include the Victoria, Edward, Kyoga, Albert, No, Tana, and Nasser. There are two main sources of the River Nile including the White Nile (from the equatorial region), and the Blue Nile (from the Ethiopian highlands). The Nile Basin covers parts of several countries (Food and Agriculture Organization FAO, 1997): Uganda (98.1 %), Kenya (8.0 %), Tanzania (8.9 %), Rwanda (75.5 %), Burundi (47.6 %), Democratic Republic of Congo (0.9 %), Sudan and South Sudan (79.0 %), Ethiopia (33.2 %), Eritrea (20.4 %), and Egypt (32.6 %). The River Nile receives little or negligible runoff from about 40 % of its drainage (basin) area which comprises dry lands of either arid or hyper-arid condition. Moreover, the River Nile loses about 50 % by evaporation in the Sudd region of South Sudan. These altogether make the Nile River to have its runoff coefficients rather lower in comparison with what would be expected from its vast drainage area.

2.2 River flow data

Monthly river flow data recorded at 18 locations (Table 1) in the Nile Basin were obtained from three sources. Flow data for 12 stations were obtained from the Global Runoff Data Centre (GRDC), Koblenz, Germany. For 2 stations, data were obtained at KU Leuven from the database of the River Nile basin Flow Regimes from International, Experimental and Network Data (FRIEND/Nile) project (http://www.unesco.org/new/en/cairo/natural-sciences/hydrology-programme/friendnile/, last access: 10 September 2014). Some flow data were obtained from the report by Kennedy & Donkin Power

Ltd (1997). The long-term average monthly flow in the last column of Table 1 is noted to range from 20 $m^3 s^{-1}$ (station 5) up to 2699 $m^3 s^{-1}$ (station 18).

2.3 Rainfall data

A number of rainfall stations were used in this study. The daily rainfall data at 5 locations over the Blue Nile were those used in a study by Taye and Willems (2013). Data for daily (monthly) rainfall at 4 (6) locations in or around Kagera (Atbara) catchment were obtained from the FRIEND/Nile project. Furthermore, daily rainfall data from 4 stations in the Kyoga Basin were obtained from the Ministry of Water and Environment, Uganda. Especially for the last two data sources, missing rainfall data records were filled-in (using the inverse distance weighted interpolation technique) in a similar way as done for a number of meteorological stations of the Nile Basin in previous studies by Onyutha and Willems (2015a, b).

Table 2 shows location and ID of the selected stations as well as the data period and long-term statistical metrics coefficient of variation (C_v), skewness (C_s) and actual excess kurtosis (C_k) for the monthly rainfall. Values of C_s and C_k greater than zero indicate that the distribution of the data deviate from the Gaussian type. The values of C_v in Kyoga and Kagera were lower than those of Atbara and Blue Nile. The highest values of C_v, C_s and K_s were obtained for stations in the Atbara catchment. This is because the catchment is located in an arid climate region and thus the data are characterized by large extent of ties caused by the existence of zeros. Moreover, the data from Atbara have larger differences between the minimum and maximum monthly rainfall totals than for other selected catchments. More monthly rainfall data series as shown in Table 3 were adopted from Onyutha and Willems (2015a).

3 Methodology

3.1 Spatial flow variation

Similarity in flow variation patterns was studied and used in a clustering procedure to group the hydrological stations. On assumption that the flow variation can be primarily explained by that in rainfall, the grouping of the stations was done based on both the seasonal and annual time scales. It is known that the rainfall in the equatorial region exhibit bimodal pattern (Nicholson, 1996). The "long-rains" and "short-rains" occur over the months of March–May (MAM) and October–December (OND) respectively. The June–September (JJAS) and January–February (JF) are dry periods. However, the rainfall in the middle section (Sudan and Ethiopia) of the River Nile Basin exhibit a unimodal pattern (Camberlin, 2009; Onyutha and Willems, 2015a) with the JJAS (MAM) as the main (slight) rainy season. The dry season is experienced over the October–February (ONDJF) period. The validity and/or consistency of the obtained groups of hydrological stations (especially with respect to regional coverage) was checked based on those formed from meteorological stations by Onyutha and Willems (2015a).

The steps taken to group the discharge stations were as follows:

i. form a common pool by putting together all the discharge stations under consideration;

ii. select a station from the pool;

iii. compute the correlation between the flow series of the selected station and the series from the other stations;

iv. form a candidate group comprising the selected station in step (ii) and all the other stations for which positive correlation was obtained in step (iii); and remove all the stations of this candidate group from the pool;

v. check that the cross-correlation coefficients between the flows of the stations in the candidate group formed in step (iv) are positive; remove and return to the

pool the station which shows negative flow cross-correlation with more than 50 % of the group members;

vi. check if the geographical locations of the stations in the candidate group are spatially coherent; remove the stations whose locations are incongruous and put them back into the pool; confirm the remaining members of the candidate group as homogenous;

vii. repeat steps (ii) to (vi) till the pool is empty.

3.2 Co-variation of flow and rainfall

In each group of the hydrological stations formed, the variation of flow was compared with that of the rainfall at both seasonal and annual time scales. This was done on a regional basis as well as at a catchment scale. For the regional basis: (1) the rainfall variation patterns at the different stations within a group (or region) were compared, (2) the variation of the region-wide rainfall average was compared with that of the region-wide mean river flow. To check on the co-variation of rainfall and flow at a catchment scale, representative catchments each with a number of meteorological stations were selected from each hydrological group formed. For each selected catchment, comparison was made between the patterns of the variation of flow at the outlet of the catchment and: (1) rainfall at each meteorological station, and (2) catchment-wide average rainfall. The idea was to assess how well, at both catchment level and regional scale, the variation in flow could be explained by that in rainfall.

3.3 Rainfall–runoff modeling

Three rainfall–runoff models including NAM, VHM and HBV were applied under the same meteorological conditions in simulating daily flows at the outlet of each selected catchment. The rainfall–runoff modeling was used to assess any possible empirical evidence for the change in catchment characteristics in the form of temporal change

in catchment runoff response to rainfall, hence between observed and simulated flow. Explanation on this idea will be given in Sect. 3.4. The selected conceptual catchment runoff models make use of the catchment-wide averaged rainfall and evaporation as their inputs to simulate the rainfall–runoff at the lumped catchment scale. To get the details on these models including the description of their model structure, variables and parameters, the reader is referred to Danish Hydraulic Institute DHI (2007), Madsen (2000) and Nielsen and Hansen (1973) (for NAM), Willems (2014), and Willems et al. (2014) (for VHM), and AghaKouchak and Habib (2010), AghaKouchak et al. (2013), and Bergström (1976) (for HBV).

For each selected catchment, the potential evaporation was computed using the FAO Penman–Monteith method (Allen et al., 1998) considering minimum and maximum temperature. The catchment-wide mean areal rainfall was calculated using the Thiessen polygon method. The calibration (validation) period of the models for each selected catchment was ensured to be at least 25 (12) years. Some of the model calibration strategies and uncertainty estimation techniques include the Generalized Likelihood Uncertainty Estimation (GLUE) (Beven and Binley, 1992), and Uncertainty Estimation based on Local Error and Clustering (UNEEC) (Solomatine and Shrestha, 2009). The UNEEC method by considering the model residuals to be indicative of the model uncertainty quantifies the uncertainty in three steps including: clustering, model error probability distribution estimation, and building model uncertainty based on the error probability distribution (Solomatine and Shrestha, 2009). As a Bayesian approach, GLUE procedure uses parameters' sets randomized from the prior distribution to infer the output (posterior) distribution based on the simulations. Because the HBV version used in this study employs the GLUE technique, GLUE was also adopted for NAM and VHM. This was for the uniformity of calibration scheme to obtain an ensemble of simulated flows from each of the models. The optimal set of parameters was considered as that with the highest Nash–Sutcliffe Efficiency (E_{NS}) (Nash and Sutcliffe, 1970). The model performance was evaluated both statistically and graphically. Statistically, the "goodness-of-fit" was evaluated in terms of the E_{NS} and the coefficient of determina-

tion (R^2). Graphically, the plots of Box–Cox (BC) transformed observed vs. simulated series were made for the maximum as well as minimum flow in each year. The BC (Box and Cox, 1964) transformation (Eq. 1) with the parameter (λ) set to 0.25 was applied to give similar weights to the maximum and minimum flows (f) so as to obtain homoscedastic model residuals. Comparison of the simulated and observed cumulative flow was also made.

$$\mathrm{BC}(f) = \frac{f^{\lambda} - 1}{\lambda} \quad (1)$$

3.4 Analyses of changes in observed and simulated overland flow

The change in catchment behavior due to the anthropogenic influence would lead to temporal change in the difference between the observed and modeled runoff flows and sub-flows. Anthropogenic influences such as deforestation, overgrazing, significant expansion of urbanized areas etc over a given catchment would: (1) affect the amount of infiltration into the soil, (2) alter the amount and velocity of the overland flow, (3) modify the rate and amount of evaporation, etc. Hence, these would alter the catchment response to the rainfall input. This difference in response should be visible through the changes in runoff volumes, sub-flow volumes, ratio between sub-flow volumes, model parameters describing the sub-flow response to such times such as the recession constant.

Because of the importance to study the runoff sub-flows and more specifically the overland flow separately, a numerical digital filter was applied to split the flow into the various sub-components. This discharge splitting was done based on the sub-flow recession constants as applied in the tool provided by Willems (2009). The temporal change in the overland flow was analyzed using two approaches including the Cumulative Rank Difference (CRD) (Onyutha, 2015) technique and the Quantile Perturbation Method (QPM) (Ntegeka and Willems, 2008; Willems, 2013). The two methods were applied to the annual maxima, annual minima and annual mean flow. Each of the two

methods CRD and QPM analyzes the given data in a different way. Whereas the CRD focuses on the cumulative effects of the variation, the QPM considers quantile changes.

The concept behind the CRD is not new as it is related to a Brownian bridge which employs the standard Brownian motion. As stated in Benson et al. (2013), a Brownian motion describes a limit Markov or memory-less process of finite-variance random walks with short-range correlation (Bhattacharya and Gupta, 1983). According to the central limit theorem, a finite-variance motion converges toward the Gaussian limit distribution (Benson et al., 2013) and this property makes the application of the Brownian motion so attractive in hydrology. The concept of the Brownian bridge in hydrology is applied in the Pettitt test (Pettitt, 1979), distribution free CUSUM test (Pages, 1954), etc, which are all important for change-point detection. However, as opposed to focusing on the change-point detection, the CRD method accumulates the difference between the exceedance and non-exceedance counts of the data points in a sample to establish periods over which the cumulative effect of the variation in the series is positive or negative. This is vital to graphically reveal hidden (short-durational) increase or decrease in the variable over unknown time periods. Such an approach falls in line with the need for graphical exploration of changes in series as opposed to the purely statistical results which might be meaningless sometimes (Kundzewicz and Robson, 2000) to an environmental practitioner. In this study, the CRD capability was deemed important to expose any persistent mismatches between the observed and modeled flow. Moreover, being rank-based, the CRD is not affected by non-normally distributed data which frequently occur in hydro-meteorology.

To apply the CRD method for sub-trend analysis, the following steps were taken:

i. rescaling of the given series in a nonparametric way using Eq. (2) to obtain the difference (D) between the exceedance and non-exceedance counts of the data points;

$$D(i) = 2R_a(i) - (n - w(i)) \quad \text{for } 1 \le i \le n \quad (2)$$

where R_a is the number of times a data point is exceeded, and w the number of times a data point appears within the given sample. To determine R_a or w, each data point is counted as if it was not considered before.

ii. calculating cumulative sum (S_m) of the rank difference using Eq. (3);

$$S_m(i) = \sum_{j=1}^{i} D(j) \quad \text{for } 1 \le i \le n \tag{3}$$

it can be checked that $\sum_{j=1}^{i} D(j)$ is always zero. $S_m(n)$ is zero as well;

iii. making the CRD plot i.e. plotting the $S_m(i)$ against the time unit of the series;

iv. identifying the sub-periods over which the series is characterized by an increasing or decreasing sub-trend.

In the CRD plot, taking $S_m = 0$ line as the reference, the values above or below this reference are considered to characterize sub-trends in the series (Onyutha, 2015). For a positive/negative trend, most if not all the scatter points in the CRD plot take the form of a curve above/below the reference. If the given series is characterized by an increasing trend in the first half and a decrease in the second half, for example, two curves are formed such that the first one (first half of the period) is above the reference and the second one below the $S_m = 0$ line (Onyutha, 2015). When there is no trend in the data, the CRD curve crosses the reference a number of times with no clear area over large time period between the curve and the $S_m = 0$ line. For a step upward/downward jump in the mean of the series (so long as there is no trend in both parts of the sub-series before and after the step jump), the scatter points take the form of two lines which meet at a point (call it the vertex) above/below the reference (Onyutha, 2015). For an upward/downward jump, the slope of the first line is positive/negative while that for the

second one is negative/positive. If the sub-series before and after the step jump all have, increasing/decreasing trends, two curves are formed above/below the reference.

Unlike the CRD method which relies on rescaled series, the QPM uses the given series directly (i.e. without rescaling) to obtain quantile anomalies. This allows the QPM outputs to be importantly applicable, for instance, in revising design quantiles to account for the decadal or multi-decadal oscillations or variability in the hydrometeorological variable. To apply the QPM, two series are derived from the same data set. One series (call it y) is the full series, and the other (denoted by x) is a sub-set extracted as a sub-period from the full series. The sub-series are contained in a moving window of a specified block length (taken as 15 years in this study). The moving window is first put at the beginning of the full time series and afterwards moved by 1 year at a time. For each moving window, quantile perturbation factors are computed as the quantiles above a selected exceedance probability threshold selected from x and divided by their corresponding counterparts from y. The ultimate anomaly for the window under consideration is determined as the average of the perturbation factors for all empirical quantiles above a given threshold. The ultimate anomalies from the different moving window positions are considered to characterize the variability of the extreme quantiles in the series. An elaborate and systematic description of the QPM can be obtained from Ntegeka and Willems (2008) and Willems (2013).

4 Results and discussions

4.1 Spatial flow variation

Two homogenous groups of the DMS were obtained based on the clustering approach. The stations numbered 1 to 9 in Table 1 (hereinafter referred to as “group 1”) are in the equatorial region and South Sudan (or more generally along the White Nile). This group comprises various main rivers and sub-basins including the Victoria Nile, Kyoga Nile, Albert Nile, Bahr El Jebel and the White Nile between Malakal and Khartoum.

The flow stations in Sudan, Ethiopia and Egypt, i.e. at the outlets of the Blue Nile and Atbara, and those along the main Nile formed "group 2" (stations numbered 10 to 18 in Table 1). Positive significant cross-correlation between the flow from the stations of each group can be seen in Tables 4 and 5 for seasonal and annual flow respectively. The correlation between the flow from a group 2 station and that from another station in group 1 was generally negative. This is illustrated using the radar plots in Fig. 2 based on annual flow. It is shown in Fig. 2a–d and e–h based on selected group 1 and 2 stations that the correlation between the annual flow of the two groups is statistically insignificant at 5 % significance level. These two DMS groups are consistent with the two homogenous regions formed by Conway and Hulme (1993) based on the inter-basin correlations of 40 year (1945–1984) precipitation and runoff data. They are the White Nile (Lake Victoria and Equatorial Lakes), and that of the Ethiopian highlands (Blue Nile and Atbara).

In another study by Nyeko-Ogiramoi et al. (2012), agglomerative hierarchical cluster algorithms to identify homogenous regions of the Nile Basin based on a combination of physiographic characteristics and hydrological properties. The authors identified 30 regions based on only catchment characteristics, and 15 considering a combination of both catchment characteristics and hydrological properties. Importantly, Nyeko-Ogiramoi et al. (2012) remarked in their conclusion that the homogenous regions were not convincing because some sub-regions were highly influenced by others especially those upstream the river based on the dependency of the flow data. This dependency of the homogenous regions on the flow data is linked to the two sources of the Nile River, which corresponds to the two groups of hydrological stations found in this study. Based on the research findings by Sestini (1993), we anticipate that the two DMS groups formed in this study follow a different spatio-temporal influence. The precipitation over the group 1 region is controlled by the changes in the equatorial circulation compared with that for group 2 which might be under the influence of the North African monsoon (Sestini, 1993).

It is important to note that the outcomes of regionalization of catchments depend on the criteria used in the grouping procedure and the intended means and purpose of the application. For a more detailed study at sub-basin level, for instance, further sub-delineation may be useful. For the Lake Victoria sub-basin, Nyeko-Ogiramoi et al. (2012) identified 5 regions to estimate flood frequency distributions from catchment characteristics. In a follow up study by Onyutha and Willems (2015c) a peak flow quantile estimation regional model was developed in a way that accounts for the spatial differences in both the physiographic characteristics and hydro-climatic properties across the sub-basin. The DMS grouping in this study was to assess the regional difference in the main flow variation attribute in the Nile Basin. Eventually, the driving forces of the rainfall variability provided also on regional basis, e.g. by Onyutha and Willems (2015a), can be linked to the DMS grouping in this study for an insight into the regional flow-rainfall co-variation.

4.2 Temporal flow variation

Figure 3 shows the temporal variations in the rescaled annual river flow. Rescaling in which each data point was divided by the sample mean was done to have comparable orders of magnitude for the flows at the different stations. The long-term mean of the rescaled flow (taken as the reference) thus has a value of one. Further confirmation of the validity of "group 1" is shown in Fig. 4 based on the co-occurrence of the long-term variation of the outflows from three lakes in the Great Lakes region (Ministry of Water, Lands and Environment MWLE, 2004). The flow of "group 1" (Fig. 3a) was above (below) the long-term reference over the period 1915–1920, mid 1960s–early 1980s (mid 1920s–late 1950s). There was a step jump in the flow mean around 1960. However, slowly over time, the equatorial region went through a recovery process to even out the effect of this step jump so as to bring the long-term mean of the Nile River flow back to its value before 1960. This recovery process was evidently still on-going even up to late 1990s (where the data used in this study ended). Figure 3b shows that the flow from "group 2" was also above the reference over the period from mid 1910s

to early 1920s. The coincidence of the rainfall total being above the reference for both groups by around 1920s could be because of the high rainfall extremes that occurred across the entire study area. For instance, on the 31 July 1920, Khartoum received daily rainfall of 88 mm which was the highest since late 1890s (Hulme and Trilsbach, 1989). However, after 1920, the flow in "group 2" was characterized by its fluctuation about the reference up to the late 1950s. From 1960 to the late 1980s, the flow was below the reference. This decrease was because of a remarkable decline in rainfall over the region. Over the Sahel region, the decline in annual rainfall was as low as 30 % over the 1970s and 1980s (Hulme, 1992).

The flows from "group 1" are noticeably different from those of "group 2" (especially after the year 1920). This is consistent with the correlation analyses given in Sect. 4.1. Related to this difference, Sestini (1993) also found that the flow from the Blue Nile is uncorrelated with that of the White Nile. However, the author found that the runoff from the Blue Nile has a moderately good correlation with the rainfall from the Sahel region. This correlation might be an indication of the close agreement between the variability patterns for the rainfall over central Ethiopia and that in central Sudan as shown by Onyutha and Willems (2015a).

4.3 Spatial rainfall variation

Recently, Onyutha and Willems (2015a) grouped meteorological stations across the study area into two and three based on the patterns of QPM anomalies and Long-Term Monthly Mean (LTMM) of rainfall respectively. Based on the QPM anomalies, the two groups included those; in the equatorial region (group A), and Ethiopia and Sudan (group B). The same groups were realized for the LTMM with the third one (group C) for the rainfall stations in Egypt. Therefore, the regional coverage of group 1 in this study is consistent with that of group A for the rainfall stations in the study by Onyutha and Willems (2015a). Moreover, the rainfall variation in group B of the cited reference was found to be in a close agreement with that of the flow for this study's group 2. The LTMM of the rainfall in Egypt is far lower (and with unclear variation patterns) than those in

groups A and B. This suggests that the influence of the rainfall over Egypt on the Nile flow is minimal.

Figure 5 shows the correlation as well as the variation of rescaled annual rainfall at selected locations within the two hydrological groups. The rainfall rescaling was done in the same way as for the flow. Figure 5a and b show close agreement between the variation of rainfall at one selected station and that of another i.e. A and B of group 1, and K and AA for group 2. Within each group, when a station was selected and the correlation between its rainfall and those at other stations computed, generally positive correlation coefficients are obtained as illustrated in Fig. 5c and d. Moreover, for the selected stations, the correlation values are statistically significant at 5 % significance level. Considering all the selected stations, the cross-correlation coefficients between the annual rainfall from one station and series of other stations are shown in Table 6 (for group 1) and Table 7 (for group 2). The close agreement between the rainfall at these various stations from each group in terms of the correlation of their QPM quantile anomalies was also demonstrated by Onyutha and Willems (2015a). However, in some few cases negative correlation was obtained between the rainfall of one station and that of another, even within the same group. This may be due to the high noise to signal ratio or spatial dissimilarity in microclimate (micro-scale features). To even out such spatial dissimilarity, the short-term fluctuations can be smoothened by averaging the temporal variation patterns of the rainfall at the various meteorological stations of each group. This was deemed vital and performed for assessing the co-variation of flow and rainfall of each group as presented next.

4.4 Co-variation of flow and rainfall

The consideration of both the regional scale and catchment level is important to provide a better understanding on the flow-rainfall co-variation. Averaging of the flow and rainfall over the entire region of each group can be considered as a means of spatial filtering of the local influences from the various stations. However, for the catchment-scale flow-rainfall co-variation, consideration was given to the flow at the catchment

outlet and catchment-wide weighted average rainfall upstream of the catchment outlet. A zoomed-in analysis such as that for the catchment-scale is important to obtain an insight into how strongly the micro-climate (micro-scale features) influence the flow-rainfall co-variation.

4.4.1 Regional scale analysis

Figure 6 shows the comparison of region-wide averaged annual flow and rainfall. The close agreement between the variation patterns of the flow series was already shown in Tables 4 and 5. It can be noticed that the pattern of the temporal flow variation is well captured by that of the rainfall in both group 1 (Fig. 6a) and 2 (Fig. 6b). Moreover, the correlation coefficient between the variation pattern of flow and rainfall for group 1 (2) was 0.56 (0.48) and statistically significant at the 5 % level based on the critical value of 0.18 (0.17). This confirmed that, on a regional basis, the variation in the flow over the selected time period can be explained by that in rainfall. Next, the validity of this confirmation was checked at a catchment level for both groups 1 and 2.

4.4.2 Catchment level analysis

Figure 7 shows the temporal variation of the annual flow at the catchment outlet and the catchment-averaged rainfall. The rainfall stations from Table 2 were used. Again, the closeness between the flow and rainfall variations is visibly evident. Further still, the correlation between rainfall and flow was significant at the 5 % level for all the selected catchments of each group, i.e. Kagera and Kyoga (Fig. 7a and b), and Blue Nile and Atbara (Fig. 7c and d).

Table 8 shows the correlation between the variation of seasonal and annual flow at the catchment outlet and the rainfall from individual stations upstream of the outlet. Although there was some anti-correlation especially in the MAM (JJAS) season for Blue Nile and Atbara (Kagera and Kyoga), generally the correlation for the annual time scale was significantly positive for all the selected catchments. This realization is also

evident for the seasons from which the variations in the annual rainfall emanate, i.e. OND (for Kagera and Kyoga) and JJAS (for Blue Nile and Atbara). Finally, it can be concluded from both the region-wide and catchment-scale analyses that the variation in seasonal and annual flow can be well explained by that in rainfall.

4.5 Rainfall runoff modeling

The main catchment within the geographical coverage of each group formed in Sect. 4.1 was selected. These are the Kagera catchment at Kyaka Ferry (60 000 km^2) and the Blue Nile catchment at Khartoum (325 000 km^2) for group 1 and 2 respectively. The three models including NAM, VHM and HBV were applied to each catchment. The calibration (validation) period of the models was 1 January 1965–31 December 1989 (1 January 1990–31 December 2002) for the Blue Nile catchment and 1 January 1950–31 December 1974 (1 January 1975–31 December 1986) for the Kagera catchment.

Figure 8 shows the time series of the observed and simulated Blue Nile and Kagera flows. The model parameters following the GLUE technique are listed in Appendix Table A1. Based on a visual judgment considering each model, better modeled results were obtained for the Blue Nile (Fig. 8a) than for the Kagera (Fig. 8b) catchment. This is because of the larger catchment size and stronger seasonal differences for the Blue Nile which leads to smoother catchment response to rainfall than that for the Kagera Basin.

Table 9 shows the statistical assessment of the models' performance. The value of both, the E_{NS} and R^2 for calibration were acceptably high. Consistent with the visual judgment from Fig. 8, the model performance (though reasonably good) in the validation was better for the Blue Nile than the Kagera catchment. For the Kagera catchment, in reference to the model calibration results, the validation E_{NS} for NAM, VHM and HBV exhibited a drop of 27, 30 and 26 % respectively. In order to check whether this drop in the E_{NS} is explained by model over-calibration, the validation input series were considered as independent model inputs and when calibration based on the GLUE scheme was repeated for this new input, there was no significant increase in the E_{NS} values

compared to those for the validation shown in Table 9. One reason for the E_{NS} drop could be the lower data quality taking into account that some measurement stations tend to be irregularly operational due to poor maintenance. Another potential reason might be the difficulty in the models to capture the dynamics of runoff generation at the catchment level as explained next. The validation period for Kagera Basin (i.e. 1975–1986) had its beginning not far from around 1960 during which the equatorial region experienced a step jump in the flow mean. It could be possible that all the models failed to adequately capture the catchment behavior in its recovery from the effect of the step jump (as seen from Figs. 3 and 4). However, because the E_{NS} values for all the models are higher than 0.5 for all the validation runs, the modeled flow was deemed adequate for the empirical investigation of the possible change in catchment rainfall–runoff response.

Figure 9 shows the graphical assessment of the goodness-of-fit between the Box–Cox transformed observed and modeled flow. Good model performance was obtained for both the annual maximum (Fig. 9d) and minimum (Fig. 9e) flows of the Kagera. For the Blue Nile, though the performance of all the models were good for the annual maxima (Fig. 9a), the HBV model tends to overestimate most of the annual minima (Fig. 9b). With respect to the cumulative flow volumes (Fig. 9c and f), the models show slight over-estimations. For Kagera catchment, the slight overestimations are due to the lower performance of the simulation results from the validation period. Note that because the Blue Nile flow has stronger seasonal variations, the flow scatter is more wide-spread for the Blue Nile (Fig. 9a and b) than for the Kagera (Fig. 9c and d). Based on these performance evaluation results, it can be generally concluded that the three models jointly allow an assessment to be made of potential temporal changes in the catchment rainfall–runoff responses.

4.6 Changes in observed and simulated overland flow

Figure 10 shows results of sub-trends in the observed and modeled overland flow. In Fig. 10a and c, it is perceptible that about half the CRD curve fell below (above) the

reference over the period 1965–1983 (1984–2000). This showed that there were both negative and positive sub-trends in the annual mean and maximum overland flows. However, the annual minimum overland flows were mainly characterized by a decrease since almost its entire CRD curve fell below the reference (Fig. 10b). The presence of a step jump in the mean flow around 1960 is evident for the Kagera (Fig. 10d–f). In the 1990s, some deviations between the modeled and observed overland annual maximum flow sub-trends (Fig. 10a) for the Blue Nile is visible for the outputs from all the models.

Figure 11 shows changes in observed and simulated overland flow in terms of the QPM quantile anomalies. For the annual maximum and mean overland flows at the Blue Nile (Fig. 11a and c), there were oscillation highs (OHs) in the mid 1960s to late 1970s, and in the 1990s. There was an oscillation low (OL) from the late 1970s to around 1990. Taye and Willems (2013) found similar results especially for the annual maximum flows in the upper Blue Nile Basin. However, for the annual minimum flows (Fig. 11b), the period from the mid 1960s to late 1970s (early 1980s to late 1990s) was characterized by an OH (OL). For Kagera, the period 1950–1959 (1960–1986) was characterized by an OL (OH) (Fig. 11d–f). Based on the QPM results, the peak of the OH was around 1965.

Consistent with the CRD sub-trend results, again some slight over- or underestimation of the observed changes was also demonstrated in the QPM anomalies. These minor discrepancies between the observed and modeled flow as demonstrated in both the CRD and QPM change detection techniques could be indicative of some possible slight changes in the catchment behavior, which may be attributed to an anthropogenic influence. A number of previous studies also ascribed hydrological changes in the different parts of the Nile Basin to anthropogenic factors. Using rainfall–runoff modelling, Legesse et al. (2004) noted a remarkable mismatch between the observed and modeled lake levels over the period 1984–1996 compared with that in 1968–1983. This discrepancy was attributable to human influence on the lake in terms of abstractions from the influent rivers (Legesse et al., 2004). According to Bewket and Sterk (2005), for the period between 1960 and 1999 there was a decrease of 0.6 mm yr^{-1} in the

Chemoga catchment flow during the dry season (October to May) probably due to an increase in cultivation area in the catchment. According to Rientjes et al. (2011), forest cover decreased from 50 to 16 % in the Gilgel Abay catchment over the period 1973–2001. They claimed this was probably due to deforestation for agriculture. Using satellite data, Elmqvist (2005) noted that the cropland area per household reduced from 0.4 to 0.1 km^2 over the period 1969–2002 in Sararya Makawi, Sudan. This decrease was probably due to an increase in the population and intensification of agriculture (Elmqvist, 2005). Based on the land-use scenario investigation using a semi-distributed hydrological model, Mango et al. (2011) concluded that the magnitude of the extreme low (high) flows would reduce (increase) if the conversion of forests to agriculture and grassland in the headwaters of the Mara catchment would continue. In the equatorial region, Olang and Fürst (2011) used rainfall–runoff modeling for 14 sub-catchments to investigate the effect of the land-use changes on the hydrology of the Nyando watershed over the period between 1973 and 2000. Although the authors found an average increase of 16 % in the peak discharges over the entire period considered, they obtained larger changes in the sub-catchments with higher deforestation rates than others.

These findings on significant catchment changes and their effects on catchment runoff flows would not be confirmed in this study. Despite the slight over- or under-estimation of the observed changes for both selected catchments, the outputs from all the models indeed exhibited close agreement in capturing the flow variability or quantile changes (by the QPM) (Fig. 11) and the cumulative effect of the flow variations or sub-trends (by the CRD approach) (Fig. 10). This generally indicates that changes in the catchment behavior in transforming the rainfall input into runoff is minimal. In related studies, similar conclusions were also made by e.g. Taye and Willems (2013) and Gebrehiwot et al. (2013), all done for the period 1960–2004. Gebrehiwot et al. (2013) applied the HBV model to the Birr, Upper-Didesa, Gilgel Abbay, and Koga catchments of the Blue Nile Basin and found that although some model parameters changed over some selected periods, the integrated functioning of the catchments showed minimal

changes. Using NAM and VHM models, Taye and Willems (2013) also concluded that there are no discernible changes noted for the Blue Nile catchment response. Therefore as shown in this study, the temporal flow variations in the Nile Basin may be attributed mainly to the rainfall variations.

5 Conclusions

This paper has assessed the main attribute of the Nile River flow variation. Based on the close agreement of the long-term temporal flow variation patterns, it was possible to group the discharge measurement stations into two; those along the White Nile i.e. from the equatorial region and South Sudan (group 1), Sudan, Ethiopia and Egypt i.e. the Blue Nile, Atbara and the main Nile (group 2).

Group 1 exhibited higher (lower) flow mean over the period from mid 1960s to early 1980s (mid 1920s to late 1950s) than that for the full period studied. From the mid 1920s to 1950s, the flow mean for group 2 was characterized by minor deviations from that of the full period (reference) considered. However, from the early1960s to late 1980s, the flow mean was lower than reference.

In order to investigate whether these flow variations are attributable to that of rainfall, the co-variation of the rainfall and flow was assessed at both the regional and catchment scale. For each hydrological region, correlation between the region-wide average rainfall and flow was computed. For the catchment-scale, four representative catchments were selected including those of the River Kagera and Lake Kyoga (for group 1), and the Blue Nile and Atbara (for group 2). Generally, there was a close agreement between the temporal variation of flow and that of rainfall. This suggested that the variation in the flows of the River Nile Basin is strongly explained by that in rainfall.

To investigate if there was any possible change in catchment behavior to interfere with the flow–rainfall relationship, three rainfall–runoff models including NAM, VHM and HBV were used to simulate runoff over two catchments each selected from one DMS group. The rainfall–runoff modeling was done under the assumption of unchang-

ing catchment characteristics over long-term data periods. The idea here was that the change in catchment behavior due to an anthropogenic influence would lead to persistent difference in the observed and modeled flows and sub-flows such as the overland sub-flow. The investigation of this deviation was made in terms of the co-occurrence of the temporal sub-trends and changes in anomalies based on the cumulative rank difference technique and the quantile perturbation method respectively. Regardless of the change detection method or rainfall–runoff model used, close agreement between the changes in observed and simulated flow was generally obtained in both selected catchments. These results suggested that the impacts of the changes in catchment behavior on the hydrology of the given catchments were nominal. This implies that the use of the variation in rainfall to explain that in the flow of the Nile Basin (especially over the selected data period) is not influenced in a significant way by the changes in catchment characteristics. The drivers of the rainfall variability for the entire Nile Basin were recently provided by Onyutha and Willems (2015a). Given that the main attribute of the flow variation is that in rainfall, indeed an insight into the prediction of flow variation can be obtained from the rainfall variability drivers. In line with this, for instance, Siam and Eltahir (2015) found it possible to obtain some logical predictive estimates of annual flows for the northern half of the Nile River based on the teleconnection between the Indian Ocean and the Nile basin. However, to reflect the difference in microclimate (micro-scale features) of the study area, it is recommended that more studies be carried on many other catchments covering the entire Nile Basin.

Acknowledgements. The research was financially supported by an IRO PhD scholarship of KU Leuven.

References

Abtew, W., Melesse, A. M., and Dessalegne, T.: El Niño Southern Oscillation link to the Blue Nile River Basin hydrology, Hydrol. Process., 23, 3653–3660, doi:10.1002/hyp.7367, 2009.

AghaKouchak, A. and Habib, E.: Application of a conceptual hydrologic model in teaching hydrologic processes, Int. J. Eng. Educ., 26, 963–973, 2010.

AghaKouchak, A., Nakhjiri, N., and Habib, E.: An educational model for ensemble streamflow simulation and uncertainty analysis, Hydrol. Earth Syst. Sci., 17, 445–452, doi:10.5194/hess-17-445-2013, 2013.

Allen, R. G., Pereira, L. S., Raes, D., and Smith, M.: Crop Evapotranspiration – Guidelines for Computing Crop Water Requirements, FAO Irrigation Drainage Paper 56, FAO – Food and Agriculture Organization of the United Nations, Rome, Italy, 1998.

Benson, D. A., Meerschaert, M. M., and Revielle, J.: Fractional calculus in hydrologic modeling: a numerical perspective, Adv. Water Resour., 51, 479–497, doi:10.1016/j.advwatres.2012.04.005, 2013.

Bergström, S.: Development and Application of a Conceptual Runoff Model for Scandinavian Catchments, SMHI RHO 7, SMHI, Norrköping, Sweden, 1976.

Beven, K. J. and Binley, A. M.: The future role of distributed models: model calibration and predictive uncertainty, Hydrol. Process., 6, 279–298, doi:10.1002/hyp.3360060305, 1992.

Bewket, W. and Sterk, G.: Dynamics in land cover and its effect on stream flow in the Chemoga watershed, Blue Nile Basin, Ethiopia, Hydrol. Process., 19, 445–458, doi:10.1002/hyp.5542, 2005.

Bhattacharya, R. and Gupta, V.: A theoretical explanation of solute dispersion in saturated porous media at the Darcy scale, Water Resour. Res., 19, 938–944, 1983.

Box, G. E. P. and Cox, D. R.: An analysis of transformations, J. Roy. Stat. Soc., 26, 211–243, 1964.

Camberlin, P.: Rainfall anomalies in the source region of the Nile and their connection with the Indian summer monsoon, J. Climate, 10, 1380–1392, 1997.

Camberlin, P.: Nile Basin climates, in: The Nile: Origin, Environments, Limnology and Human Use, Monographiae Biologicae, vol. 89, edited by: Dumont, H. J., Springer, Dordrecht, 307–333, 2009.

Conway, D. and Hulme, M.: Recent fluctuations in precipitation and runoff over the Nile subbasins and their impact on main Nile discharge, Climatic Change, 25, 127–151, 1993.

DHI: MIKE11 – A Modeling System for Rivers and Channels, Reference Manual, DHI water & environment, Hørsholm, Denmark, 278–325, 2007.
Elmqvist, B.: Land use assessment in the drylands of Sudan using historical and recent high resolution satellite data, in: The 31st International Symposium on Remote Sensing of the Environment, June 2004, ISRSE, St. Petersburg, 2005.
FAO: Irrigation Potential in Africa: a Basin Approach, 4, M-54, FAO Land and Water Bull., Rome, Italy, 1997.
Gebrehiwot, S. G., Seibert, J., Gärdenäs, A. I., Mellander, P.–E., and Bishop, K.: Hydrological change detection using modeling: half a century of runoff from four rivers in the Blue Nile Basin, Water Resour. Res., 49, 3842–3851, doi:10.1002/wrcr.20319, 2013.
Hulme, M.: Rainfall changes in Africa: 1931–1960 to 1961–1990, Int. J. Climatol., 12, 685–699, 1992.
Hulme, M. and Trilsbach, A.: The August 1988 storm over Khartoum: its climatology and impact, Weather, 44, 82–90, 1989.
Kennedy & Donkin Power Ltd in Association with Sir Alexander Gibb & Partners and Kananura Melvin Consulting Engineers: Hydropower Development Plan Part 1 (Final Report) – Vol. 8, and Environmental Impact Assessment (Stage 1) – Vol. 8, Uganda Electricity Board, Kampala, Uganda, 1997.
Kundzewicz, Z. W. and Robson, A.: Detecting Trend and Other Changes in Hydrological Data, World Climate Program – Water, WMO/UNESCO, WCDMP-45, WMO/TD 1013, WMO, Geneva, 157 pp., 2000.
Legesse, D., Vallet-Coulomba, C., and Gasse, F.: Hydrological response of a catchment to climate and land use changes in tropical Africa: case study south central Ethiopia, J. Hydrol., 275, 67–85, doi:10.1016/S0022-1694(03)00019-2, 2003.
Legesse, D., Vallet-Coulomb, C., and Gasse, F.: Analysis of the hydrological response of a tropical terminal lake, Lake Abiyata (Main Ethiopian Rift Valley) to changes in climate and human activities, Hydrol. Process., 18, 487–504, doi:10.1002/hyp.1334, 2004.
Madsen, H.: Automatic calibration of a conceptual rainfall–runoff model using multiple objectives, J. Hydrol., 235, 276–288, doi:10.1016/S0022-1694(00)00279-1, 2000.
Mango, L. M., Melesse, A. M., McClain, M. E., Gann, D., and Setegn, S. G.: Land use and climate change impacts on the hydrology of the upper Mara River Basin, Kenya: results of a modeling study to support better resource management, Hydrol. Earth Syst. Sci., 15, 2245–2258, doi:10.5194/hess-15-2245-2011, 2011.

MWLE: The Year-Book of Water Resource Managagement Department 2002–2003, Sub–Sector Reform Study Report, Ministry of Water, Lands and Environment (MWLE), Entebbe, Uganda, 2004.
Nash, J. E. and Sutcliffe, J. V.: River flow forecasting through conceptual models part I – a discussion of principles, J. Hydrol., 10, 282–290, doi:10.1016/0022-1694(70)90255-6, 1970.
Nicholson, S. E.: A review of climate dynamics and climate variability in eastern Africa, in: The Limnology, Climatology and Paleoclimatology of the East African Lakes, edited by: Johnson, T. C. and Odada, E. O., Gordon and Breach, Amsterdam, the Netherlands, 25–56, 1996.
Nielsen, S. A. and Hansen, E.: Numerical simulation of the rainfall–runoff process on a daily basis, Nord. Hydrol., 4, 171–190, 1973.
Ntegeka, V. and Willems, P.: Trends and multidecadal oscillations in rainfall extremes, based on a more than 100 year time series of 10 min rainfall intensities at Uccle, Belgium, Water Resour. Res., 44, W07402, doi:10.1029/2007WR006471, 2008.
Nyeko-Ogiramoi, P., Willems, P., Mutua, F. M., and Moges, S. A.: An elusive search for regional flood frequency estimates in the River Nile basin, Hydrol. Earth Syst. Sci., 16, 3149–3163, doi:10.5194/hess-16-3149-2012, 2012.
Olang, L. O. and Fürst, J.: Effects of land cover change on flood peak discharges and runoff volumes: model estimates for the Nyando River Basin, Kenya, Hydrol. Process., 25, 80–89, doi:10.1002/hyp.7821, 2011.
Onyutha, C.: Identification of sub-trends from hydro-meteorological series, Stoch. Environ. Res. Risk A, doi:10.1007/s00477-015-1070-0, in press, 2015.
Onyutha, C. and Willems, P.: Spatial and temporal variability of rainfall in the Nile Basin, Hydrol. Earth Syst. Sci., 19, 2227–2246, doi:10.5194/hess-19-2227-2015, 2015a.
Onyutha, C. and Willems, P.: Uncertainty in calibrating generalised Pareto distribution to rainfall extremes in Lake Victoria Basin, Hydrol. Res., 46, 356–376, doi:10.2166/nh.2014.052, 2015b.
Onyutha, C. and Willems, P.: Empirical statistical characterization and regionalization of amplitude–duration–frequency curves for extreme peak flows in the Lake Victoria Basin, East Africa, Hydrolog. Sci. J., 60, 997–1012, doi:10.1080/02626667.2014.898846, 2015c.
Page, E. S.: Continuous inspection schemes, Biometrika, 41, 100–115, 1954.
Pettitt, A. N.: A non-parametric approach to the change-point problem, J. Roy. Stat. Soc. C, 28, 126–135, 1979.

Rientjes, T. H. M., Haile, A. T., Kebede, E., Mannaerts, C. M. M., Habib, E., and Steenhuis, T. S.: Changes in land cover, rainfall and stream flow in Upper Gilgel Abbay catchment, Blue Nile basin – Ethiopia, Hydrol. Earth Syst. Sci., 15, 1979–1989, doi:10.5194/hess-15-1979-2011, 2011.

Sestini, G.: Implications of climatic changes for the Nile Delta, in: Climatic Change in the Mediterranean, edited by: Sestini, G., Edward Arnold Publisher, London, 535–601, 1993.

Siam, M. S. and Eltahir, E. A. B.: Explaining and forecasting interannual variability in the flow of the Nile River, Hydrol. Earth Syst. Sci., 19, 1181–1192, doi:10.5194/hess-19-1181-2015, 2015.

Solomatine, D. P. and Shrestha, D. L.: A novel method to estimate model uncertainty using machine learning techniques, Water Resour. Res., 45, W00B11, doi:10.1029/2008WR006839, 2009.

Taye, M. T. and Willems, P.: Identifying sources of temporal variability in hydrological extremes of the Upper Blue Nile Basin, J. Hydrol., 499, 61–70, doi:10.1016/j.jhydrol.2013.06.053, 2013.

Tierney, J. E., Smerdon, J. E., Anchukaitis, K. J., and Seager, R.: Multidecadal variability in East African hydroclimate controlled by the Indian Ocean, Nature, 493, 389–392, doi:10.1038/nature11785, 2013.

Willems, P.: A time series tool to support the multi-criteria performance evaluation of rainfall–runoff models, Environ. Model. Softw., 24, 311–321, doi:10.1016/j.envsoft.2008.09.005, 2009.

Willems, P.: Multidecadal oscillatory behaviour of rainfall extremes in Europe, Climatic Change, 120, 931–944, doi:10.1007/s10584-013-0837-x, 2013.

Willems, P.: Parsimonious rainfall–runoff model construction supported by time series processing and validation of hydrological extremes – Part 1: Step-wise model-structure identification and calibration approach, J. Hydrol., 510, 578–590, doi:10.1016/j.jhydrol.2014.01.017, 2014.

Willems, P., Mora, D., Vansteenkiste, T., Taye, M. T., and Van Steenbergen, N.: Parsimonious rainfall–runoff model construction supported by time series processing and validation of hydrological extremes – Part 2: Intercomparison of models and calibration approaches, J. Hydrol., 510, 591–609, doi:10.1016/j.jhydrol.2014.01.028, 2014.

Table 1. Overview of the selected hydrological stations and monthly flow data.

St. no.	Name	Nile Region	Country	Long. [°]	Lat. [°]	Data Period	AF [$m^3 s^{-1}$]
1	Kyaka Ferry	L. Vict. Basin	Tanzania	31.42	−1.27	1940–1971	194
2	Jinja	Victoria Nile	Uganda	33.20	0.43	1946–1970	909
3	Paara	Victoria Nile	Uganda	31.57	2.28	1948–1970	946
4[a]	Kamdini	Kyoga Nile	Uganda	32.33	2.24	1950–2000	1075
5[b]	Kafu	Victoria Nile	Uganda	32.05	1.55	1953–1970	20
6[b]	Aswa	Victoria Nile	Uganda	32.35	2.57	1948–1968	37
7	Panyango	Albert Nile	Uganda	31.65	2.65	1948–1970	1079
8	Mongalla	White Nile	South Sudan	31.77	5.20	1912–1982	1050
9	Malakal	White Nile	South Sudan	31.62	9.58	1912–1982	939
10	Sennar	Blue Nile	Sudan	33.58	13.57	1912–1982	1438
11[c]	Khartoum	Blue Nile	Sudan	32.51	15.64	1900–1982	1564
12[b]	El Diem	Blue Nile	Sudan	34.93	11.24	1964–2005	1500
13[b]	Babu	Blue Nile	Ethiopia	38.62	10.08	1968–1998	39
14	Kilo 3	Atbara	Sudan	33.99	17.68	1912–1982	385
15	Tamaniat	Main Nile	Sudan	32.56	15.95	1911–1982	2349
16	Hud. + Hass.	Main Nile	Sudan	33.95	17.59	1908–1982	2386
17	Dongola	Main Nile	Sudan	30.49	19.18	1912–1984	2622
18	Aswan Dam	Main Nile	Egypt	32.90	23.96	1900–1965	2699

[a] the source of data is Kennedy & Donkin Power Ltd (1997).
[b] the source of data is FRIEND/Nile; Hud. + Hass.: Hudeiba + Hassanab.
[c] data obtained based on personal connection.
AF: average of the monthly flow.
L. Vict.: Lake Victoria.
Long.: Longitude.
Lat.: Latitude.
Data for unmarked stations were obtained from the Global Runoff Data Center (GRDC).

Table 2. Daily rainfall stations for selected catchments.

Station Paper ID	Name	Location Long.	Lat.	Data period From	To	Statistical metric C_k [–]	C_s [–]	C_v [–]
Kagera Basin								
Kag1	Mugera (Paroisse)	29.97	−3.32	1940	1990	0.98	0.73	0.78
Kag2	Muyinga	30.35	−2.85	1940	1992	−0.17	0.44	0.72
Kag3	Igabiro Estate	31.55	−1.82	1940	1994	0.47	0.78	0.80
Kag4	Musenyi (Paroisse)	30.03	−2.97	1940	1994	1.34	1.06	0.83
Atbara catchment								
Atb1	Atbara	33.97	17.70	1907	1995	36.39	5.18	3.06
Atb2	Ungwatiri	36.00	16.90	1950	1981	22.60	4.26	2.66
Atb3	Abu-Quta	32.70	14.88	1948	1987	8.65	2.81	2.06
Atb4	Haiya	36.37	18.33	1950	1981	33.39	5.10	2.67
Atb5	Gedaref	35.40	14.03	1903	1996	3.07	1.78	1.50
Atb6	Ghadambaliya	34.98	14.20	1948	1988	3.88	1.95	1.65
Blue Nile Basin								
Blu1	Bahr Dar	37.41	11.60	1964	2004	0.95	1.36	1.30
Blu2	Debremarcos	37.67	10.33	1964	2004	−0.46	0.86	1.00
Blu3	Gonder	37.40	12.55	1964	2004	1.54	1.44	1.21
Blu4	Addis Ababa	38.75	09.03	1964	2004	−0.06	0.95	1.02
Blu5	Kombolcha	39.83	11.10	1964	2004	2.32	1.56	1.11
Kyoga Basin								
Kyo1	Imanyiro	33.27	0.29	1950	1977	3.51	1.34	0.65
Kyo2	Kapchorwa	34.43	1.24	1950	1995	3.07	1.15	0.69
Kyo3	Buwabwale	34.21	0.54	1950	1977	4.73	1.61	0.69
Kyo4	Ivukula	33.35	0.57	1950	1997	2.12	1.24	0.68

Long. and Lat. stand for longitude [°] and latitude [°] respectively.

Table 3. Monthly rainfall stations adopted from Onyutha and Willems (2015a).

SNo.	Station	Paper ID	Long.	Lat.	SNo.	Station	Paper ID	Long.	Lat.
1	Kabale	A	29.98	−1.25	18	Kassala	R	36.40	15.47
2	Namasagali	B	32.93	1.00	19	Kubbum	S	23.77	11.78
3	Igabiro	C	31.53	−1.78	20	Kutum	T	24.67	14.20
4	Kibondo	D	30.68	−3.57	21	Nyala	U	24.88	12.05
5	Ngudu	E	33.33	−2.93	22	Renk	V	32.78	11.75
6	Shanwa	F	33.75	−3.15	23	Shambat-Obs.	W	32.53	15.67
7	Tarime	G	34.37	−1.35	24	Shendi	X	33.43	16.70
8	Bujumbura	H	29.32	−3.32	25	Talodi	Y	31.38	10.60
9	El-Da-Ein	I	26.10	11.38	26	Talodi-M-Agr.	Z	30.50	10.60
10	El-Fasher	J	25.33	13.62	27	Umm-Ruwaba	AA	31.20	12.80
11	El-Obeid	K	30.23	13.17	28	Wau	AB	28.02	7.70
12	En-Nahud	L	28.43	12.70	29	Combolcha	AC	39.72	11.08
13	Er-Rahad	M	30.60	12.70	30	Debremarcos	AD	37.72	10.35
14	Fashashoya	N	32.50	13.40	31	Gambela	AE	34.58	8.25
15	Garcila	O	23.12	12.35	32	Gore	AF	35.55	8.17
16	Hawata	P	34.60	13.40	33	Wenji	AG	39.25	8.42
17	Jebelein	Q	32.78	12.57					

Long.: longitude [°].
Lat.: latitude [°].

Table 4. Correlation between seasonal flow series from the different stations.

Group 1									
Station	1	2	3	4	5	6	7	8	9
1	–	***0.890***	***0.888***	***0.886***	***0.899***	*0.426*	***0.843***	***0.844***	***0.702***
2	**0.896**	–	***0.983***	***0.987***	***0.734***	*0.336*	***0.961***	***0.969***	***0.857***
3	**0.896**	**0.992**	–	***0.996***	***0.758***	*0.341*	***0.946***	***0.965***	***0.885***
4	**0.892**	**0.988**	**0.993**	–	***0.763***	*0.378*	***0.959***	***0.971***	***0.874***
5	**0.885**	**0.705**	**0.728**	**0.751**	–	***0.600***	***0.778***	***0.743***	***0.597***
6	0.430	0.192	0.220	0.265	**0.601**	–	***0.470***	*0.427*	*0.354*
7	**0.884**	**0.923**	**0.938**	**0.937**	**0.807**	0.315	–	***0.954***	***0.873***
8	**0.877**	**0.972**	**0.981**	**0.978**	**0.804**	0.294	**0.949**	–	***0.822***
9	**0.633**	**0.898**	**0.902**	**0.888**	**0.540**	0.121	**0.859**	**0.837**	–
Group 2									
Station	10	11	12	13	14	15	16	17	18
10	–	***0.969***	***0.978***	***0.423***	***0.735***	***0.929***	***0.900***	***0.921***	***0.882***
11	**0.854**	–	***0.961***	*0.340*	***0.760***	***0.950***	***0.907***	***0.930***	***0.890***
12	**0.513**	**0.525**	–	***0.486***	***0.822***	***0.874***	***0.940***	***0.949***	***0.992***
13	0.269	**0.443**	**0.827**	–	***0.434***	*0.268*	*0.319*	***0.371***	NA
14	0.159	0.238	0.214	0.025	–	***0.741***	***0.680***	***0.811***	***0.780***
15	0.215	0.288	**0.506**	**0.473**	0.318	–	***0.910***	***0.935***	***0.913***
16	0.222	0.317	**0.450**	**0.369**	0.337	**0.968**	–	***0.935***	***0.837***
17	0.189	0.243	0.343	**0.543**	0.295	**0.959**	**0.948**	–	***0.968***
18	0.231	0.135	**0.994**	NA	0.296	**0.873**	**0.780**	**0.919**	–

Note: (1) Italicized (un-italicized) correlation values above (below) the diagonal cells (–) are for the JJAS (MAM) seasonal flow.
(2) NA: data time periods of the stations do not overlap and thus no correlation values.
(3) Bold values are significant at 5 % level.

Table 5. Correlation between annual flow series from the different stations.

			Flow station								
	G1		1	2	3	4	5	6	7	8	9
		G2	10	11	12	13	14	15	16	17	18
Flow station	1	10	–	***0.903***	***0.890***	***0.897***	***0.838***	***0.487***	***0.879***	***0.873***	***0.740***
	2	11	**0.982**	–	***0.989***	***0.988***	***0.768***	*0.392*	***0.961***	***0.980***	***0.871***
	3	12	**0.977**	**0.966**	–	***0.998***	***0.810***	*0.438*	***0.960***	***0.988***	***0.886***
	4	13	**0.365**	0.314	**0.434**	–	***0.825***	*0.456*	***0.968***	***0.987***	***0.884***
	5	14	**0.764**	**0.796**	**0.874**	0.335	–	***0.791***	***0.880***	***0.830***	***0.710***
	6	15	**0.895**	**0.896**	**0.840**	0.322	**0.689**	–	***0.567***	***0.491***	*0.446*
	7	16	**0.857**	**0.867**	**0.898**	0.279	**0.659**	**0.933**	–	***0.975***	***0.896***
	8	17	**0.928**	**0.929**	**0.917**	0.249	**0.783**	**0.964**	**0.941**	–	***0.895***
	9	18	**0.837**	**0.864**	**0.825**	NA	**0.747**	**0.914**	**0.839**	**0.952**	–

Note: (1) Italicized and un-italicized correlation values above (below) the diagonal cells (–) are for the group 1 (G1) and group 2 (G2) respectively.
(2) NA: data time periods of the stations do not overlap and thus no correlation.
(3) Bold values are significant at 5 % level.

Table 6. Correlation between annual or MAM rainfall from the different stations in group 1 region.

Station	A	B	C	D	E	F	G	H
A	–	*0.22*	*0.01*	***0.34***	*0.13*	***0.37***	*0.18*	*0.21*
B	**0.56**	–	*0.11*	*0.23*	*−0.02*	*0.24*	*0.14*	*0.14*
C	**0.27**	**0.30**	–	*0.26*	*0.14*	*0.03*	*0.05*	***0.29***
D	0.12	0.25	**0.33**	–	***0.31***	***0.29***	***0.32***	*0.25*
E	**0.52**	**0.44**	**0.55**	**0.42**	–	***0.44***	*0.28*	*−0.18*
F	**0.39**	**0.39**	**0.40**	**0.42**	**0.67**	–	*0.22*	*0.03*
G	**0.34**	**0.36**	**0.33**	**0.42**	**0.64**	**0.53**	—	*0.15*
H	0.08	0.01	0.15	0.26	0.13	0.08	0.19	–

Note: (1) Italicized (un-italicized) correlation values above (below) the diagonal cells (–) are for the MAM (annual) rainfall.
(2) Bold values are significant at 5 % level.

Table 7. Correlation between annual or JJAS rainfall from the different stations in group 2 region.

Station	I	J	K	L	M	N	O	P	Q	R	S	T	U	V	W	X	Y	Z	AA	AB	AC	AD	AE	AF	AG
I	–	***0.55***	***0.49***	***0.58***	*0.24*	***0.32***	***0.37***	***0.30***	*0.25*	*0.15*	***0.33***	***0.58***	***0.55***	*0.26*	***0.34***	***0.51***	*0.17*	***0.44***	***0.39***	***0.30***	***0.45***	***0.54***	***0.40***	*0.06*	*−0.16*
J	**0.59**	–	***0.39***	***0.34***	***0.28***	*0.29*	*0.29*	*0.25*	***0.38***	*0.15*	***0.51***	***0.71***	***0.58***	*0.18*	***0.42***	***0.59***	*0.16*	***0.37***	***0.32***	*0.12*	***0.53***	*0.13*	*0.17*	*0.10*	*−0.01*
K	**0.46**	**0.39**	–	***0.43***	***0.42***	***0.47***	***0.47***	***0.33***	***0.39***	*0.19*	***0.44***	***0.49***	***0.37***	*0.16*	***0.32***	***0.37***	*0.12*	***0.20***	***0.67***	*0.07*	***0.42***	*−0.25*	***0.31***	*−0.17*	*−0.01*
L	**0.61**	**0.40**	**0.43**	–	*0.20*	***0.43***	***0.30***	*0.14*	***0.27***	*0.18*	***0.43***	***0.43***	***0.50***	*0.18*	***0.29***	***0.34***	*0.06*	***0.38***	***0.29***	***0.25***	***0.43***	*0.16*	*0.13*	*−0.02*	***−0.31***
M	**0.34**	**0.33**	**0.44**	**0.26**	–	***0.47***	***0.38***	*0.16*	***0.52***	*0.26*	***0.38***	***0.46***	***0.37***	*0.16*	*0.27*	*0.25*	***0.28***	***0.46***	***0.46***	*0.21*	*0.30*	*−0.04*	*0.21*	*−0.08*	*0.19*
N	0.26	**0.26**	**0.47**	**0.45**	**0.46**	–	*0.31*	*0.08*	***0.38***	*0.18*	***0.43***	***0.42***	***0.50***	***0.33***	***0.49***	***0.31***	*0.02*	*0.18*	***0.50***	*0.07*	***0.42***	*0.20*	*0.14*	*−0.04*	*−0.11*
O	**0.40**	**0.30**	**0.49**	**0.34**	**0.50**	**0.32**	–	***0.44***	*0.14*	*0.24*	***0.45***	***0.53***	***0.50***	*0.25*	*0.26*	***0.46***	*0.27*	***0.36***	***0.69***	*0.20*	*0.28*	*0.03*	***0.45***	*0.11*	*−0.19*
P	**0.30**	**0.30**	**0.35**	0.21	0.11	0.06	**0.50**	–	*0.14*	*0.08*	***0.43***	***0.44***	***0.46***	*0.25*	***0.32***	*0.29*	*0.22*	*0.14*	***0.48***	*0.12*	*0.28*	*−0.10*	*0.26*	*0.26*	*0.15*
Q	**0.32**	**0.39**	**0.33**	**0.32**	**0.51**	**0.32**	0.13	0.10	–	*0.18*	***0.38***	***0.38***	***0.48***	***0.30***	***0.36***	*0.28*	*0.07*	***0.30***	***0.36***	*0.08*	***0.37***	*0.23*	*0.18*	*0.20*	***0.40***
R	**0.24**	0.20	**0.26**	**0.22**	**0.28**	0.18	0.28	0.08	0.13	–	***0.32***	*0.24*	*0.19*	*0.03*	*0.02*	*0.12*	*0.09*	*0.21*	*0.15*	*0.09*	*0.09*	*−0.10*	*0.11*	*0.14*	*−0.03*
S	**0.36**	**0.51**	**0.37**	**0.47**	**0.41**	**0.38**	**0.45**	**0.49**	**0.36**	**0.41**	–	***0.62***	***0.61***	***0.44***	***0.35***	***0.33***	*0.16*	*0.25*	***0.54***	*0.01*	***0.41***	*−0.08*	*0.19*	*0.19*	*−0.15*
T	**0.57**	**0.73**	**0.48**	**0.47**	**0.49**	**0.42**	**0.52**	**0.46**	**0.41**	**0.31**	**0.65**	–	***0.68***	***0.29***	***0.58***	***0.64***	*0.19*	***0.45***	***0.45***	***0.31***	***0.63***	*0.09*	***0.31***	*0.10*	*0.07*
U	**0.56**	**0.62**	**0.37**	**0.46**	**0.41**	**0.51**	**0.50**	**0.52**	**0.42**	0.22	**0.61**	**0.71**	–	*0.24*	***0.49***	***0.47***	*0.11*	***0.42***	***0.47***	***0.31***	***0.52***	*0.03*	*0.31*	*0.30*	*0.06*
V	**0.27**	0.23	0.21	0.19	**0.30**	0.26	**0.37**	**0.36**	**0.29**	0.03	**0.52**	**0.33**	**0.32**	–	*0.17*	*0.23*	*0.24*	*0.28*	*0.28*	*0.02*	***0.53***	*0.11*	*0.22*	*−0.15*	*0.14*
W	0.15	**0.46**	**0.28**	**0.23**	0.14	**0.36**	0.09	0.20	**0.29**	−0.01	0.24	**0.50**	**0.50**	0.13	–	***0.58***	*0.13*	*0.23*	*0.27*	*0.23*	***0.50***	*−0.08*	*0.05*	*0.10*	*0.00*
X	**0.34**	**0.43**	**0.43**	**0.34**	0.19	**0.35**	**0.39**	0.28	0.16	0.15	0.25	**0.46**	**0.36**	**0.35**	**0.45**	–	*0.27*	***0.50***	***0.37***	***0.35***	***0.46***	***0.43***	*0.18*	*−0.03*	*−0.17*
Y	**0.32**	0.21	0.22	0.22	**0.33**	0.08	**0.42**	**0.35**	0.09	0.13	0.25	**0.28**	0.19	**0.28**	0.15	**0.25**	–	***0.63***	*0.11*	*0.08*	*0.28*	*−0.11*	*0.13*	*−0.05*	*−0.03*
Z	**0.61**	**0.40**	**0.33**	**0.48**	**0.47**	0.23	**0.57**	0.29	0.26	0.21	**0.32**	**0.50**	**0.55**	**0.33**	0.10	**0.39**	**0.65**	–	*0.25*	***0.38***	***0.40***	*0.26*	*0.19*	*−0.06*	*0.04*
AA	**0.36**	**0.34**	**0.65**	**0.31**	**0.51**	**0.55**	**0.62**	**0.41**	**0.35**	0.24	**0.45**	**0.42**	**0.48**	**0.39**	**0.28**	**0.44**	0.20	**0.34**	–	*0.09*	***0.39***	*−0.28*	***0.33***	*−0.03*	*0.09*
AB	**0.44**	**0.33**	0.13	**0.32**	**0.27**	0.20	0.28	0.14	0.24	0.17	0.22	**0.34**	**0.39**	0.12	**0.30**	**0.31**	**0.26**	**0.67**	0.14	–	*0.25*	*0.29*	*0.25*	*0.07*	*0.25*
AC	**0.42**	**0.29**	0.24	**0.31**	0.29	**0.33**	0.18	0.24	**0.40**	0.22	0.29	**0.49**	**0.38**	**0.40**	**0.52**	**0.41**	0.19	0.30	0.25	**0.37**	–	***0.35***	***0.35***	*0.07*	*0.07*
AD	0.15	0.05	−0.24	0.14	−0.02	0.10	−0.18	−0.09	0.22	0.02	−0.16	0.26	−0.06	0.07	0.07	0.05	0.11	−0.03	**−0.35**	0.22	0.18	–	*0.12*	*0.15*	*0.23*
AE	**0.40**	**0.25**	**0.35**	0.15	**0.34**	0.24	**0.40**	0.28	**0.25**	0.16	0.19	**0.39**	**0.40**	**0.32**	0.17	**0.31**	0.23	**0.45**	**0.31**	**0.38**	0.14	0.10	–	*0.04*	*0.22*
AF	0.10	0.11	−0.14	−0.07	−0.01	0.04	0.18	**0.30**	**0.35**	0.13	0.23	0.15	**0.38**	−0.02	**0.30**	−0.01	−0.02	0.09	0.04	**0.35**	0.22	0.16	0.24	–	*−0.02*
AG	−0.23	−0.12	−0.22	**−0.40**	0.12	−0.25	−0.24	−0.03	**0.37**	0.01	−0.10	0.01	−0.02	0.08	0.00	**−0.26**	−0.18	−0.16	−0.02	0.12	0.15	**0.44**	0.11	0.13	–

Note: (1) Italicized (un-italicized) correlation values above (below) the diagonal cells (–) are for the JJAS (annual) rainfall.
(2) Bold values are significant at 5 % level.

Table 8. Correlation between the variation of rainfall and river flows.

Rainfall	MAM	JJAS	ONDJF	Annual	Rainfall	MAM	JJAS	OND	Annual
	Blue Nile Basin {0.28}					Kyoga Basin {0.24}			
Blu1	−0.04	**0.29**	**0.62**	**0.34**	Kyo1	**0.28**	−0.12	**0.27**	**0.32**
Blu2	−0.11	**0.34**	**0.57**	**0.32**	Kyo2	**0.25**	0.04	**0.26**	**0.41**
Blu3	−0.21	**0.47**	**0.53**	**0.50**	Kyo3	0.23	0.13	**0.36**	**0.36**
Blu4	0.10	**0.46**	0.09	**0.31**	Kyo4	0.21	0.12	**0.36**	**0.40**
Blu5	−0.15	**0.69**	0.26	**0.55**	BW	**0.32**	0.06	**0.38**	**0.46**
BW	−0.12	**0.69**	**0.59**	**0.68**					
Atbara catchment					Kagera Basin {0.28}				
Abt1	−0.06	**0.37**	−0.06	**0.36**	Kag1	**0.38**	0.12	**0.36**	**0.64**
Abt2	−0.16	**0.44**	0.06	**0.44**	Kag2	0.11	0.24	**0.52**	**0.54**
Abt3	−0.09	**0.59**	−0.08	**0.58**	Kag3	0.06	−0.14	**0.34**	**0.29**
Abt4	−0.24	**0.57**	0.01	**0.61**	Kag4	**0.37**	0.21	**0.39**	**0.53**
Abt5	−0.02	**0.36**	0.11	**0.35**	BW	0.34	0.18	**0.60**	**0.72**
Abt6	0.12	**0.42**	−0.03	**0.38**					
CW	−0.04	**0.42**	0.05	**0.40**					

Bold values are significant at 5 % level.
CW: catchment-wide.
BW: basin-wide.
The value in { } denotes the correlation critical value at the significance level of 5 %. The critical values for Atbara catchment were 0.22 (Abt1), 0.37 (Abt2), 0.35 (Abt3), 0.37 (Abt4), 0.22 (Abt5), 0.35 (Abt6), and 0.22 (CW).

Table 9. Statistical measures of the agreement between the observed and simulated flows for the Blue Nile and Kagera catchments.

Model	Blue Nile		Kagera	
	E_{NS}	R^2	E_{NS}	R^2
Calibration				
VHM	0.74	0.77	0.77	0.82
HBV	0.79	0.81	0.72	0.81
NAM	0.77	0.79	0.70	0.80
Validation				
VHM	0.73	0.76	0.54	0.59
HBV	0.72	0.77	0.53	0.61
NAM	0.74	0.75	0.51	0.60

Table A1. List of model parameters after calibration.

VHM		Blue Nile	Kagera
Soil moisture (storage) sub-model			
Maximum soil water content:	U_{max} (mm)	1950	2420
Soil water content at maximum evapotranspiration:	U_{evap} (mm)	300	964
Initial soil water content:	U_{init} (mm)	650	20
Model coefficients:	c_1	1.0	0.9
	c_2	0.67	0.1
Overland flow sub-model			
Model coefficients:	c_1	−11.07	−7.09
	c_2	−0.35	2.93
	c_3	0.55	0.99
	c_4	3.12	0.82
Interflow sub-model			
Model coefficients:	c_1	−8.99	−9.3
	c_2	−1.33	0.43
	c_3	−0.15	0.65
	c_4	3.12	3.32
Flow routing recession constant			
Base flow:	K_B (day)	120	50
Interflow:	K_I (day)	40	40
Overland flow:	K_O (day)	20	20
HBV model			
Degree Day factor	D_D (mm °C^{-1} day^{-1})	5.84	5.72
Shape coefficient	β (–)	4.32	1.04
Model parameter	c (°C^{-1})	0.07	0.07
Field capacity	F_C (mm)	171.52	1058.65
Soil permanent wilting point	P_{wp} (mm)	97.63	130.08
Near surface flow storage coefficient	K_0 (day^{-1})	0.08	0.06
Threshold water level	T_{WL} (mm)	2.23	2.27
Interflow storage coefficient	K_1 (day^{-1})	0.03	0.05
Baseflow storage coefficient	K_2 (day^{-1})	0.02	0.02
Percolation storage coefficient	K_p (day^{-1})	0.04	0.11
NAM model			
Maximum soil water content in the surface storage	U_{max} (mm)	40	0.72
Maximum soil water content in lower zone storage	L_{max} (mm)	250	0.25
Time constant for overland flow	CQ_{OF} (day)	0.3	0.01
Time constant for interflow	CK_{IF} (day)	600	20
Time constant for overland and interflow routing	$CK_{1,2}$ (day)	34	400
Time constant for baseflow	CK_{BF} (day)	4000	4000
Threshold for overland flow	T_{OF}	0.23	0.2
Threshold for interflow	T_{IF}	0.1	0.5
Threshold for groundwater recharge	T_G	0.2	0.4

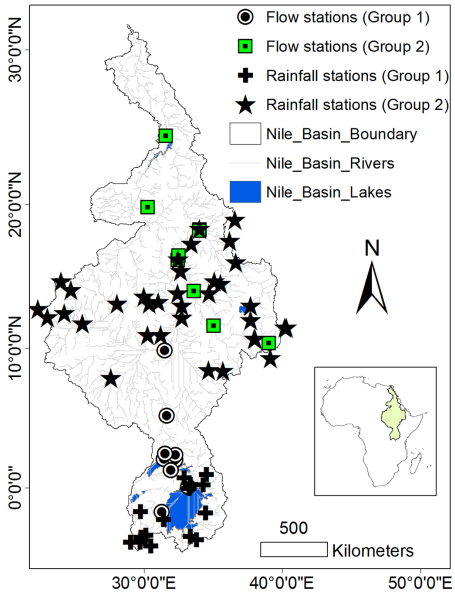

Figure 1. Locations of the selected hydrological and meteorological stations (see Tables 1 and 2 for details) in the Nile Basin.

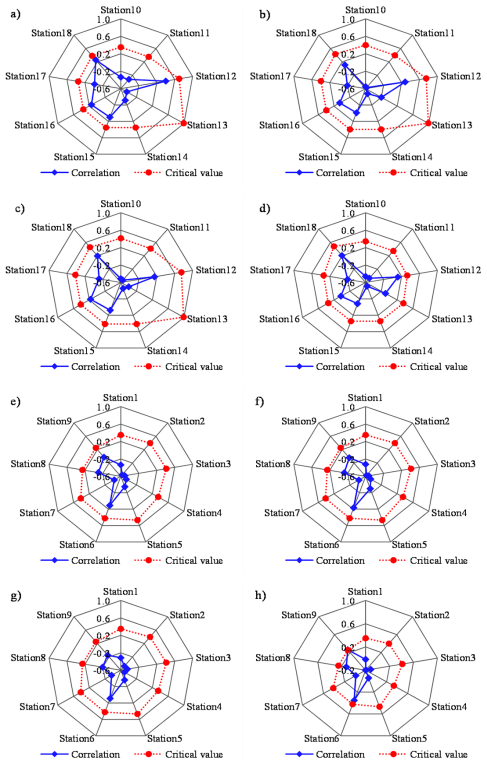

Figure 2. Correlation between annual flow of group 2 and that for group 1 station **(a)** 1, **(b)** 2, **(c)** 3 and **(d)** 4; and correlation between flow of group 1 and that for group 2 station **(e)** 10, **(f)** 11, **(g)** 14 and **(h)** 17. The critical values of each chart are at significance level of 5 %.

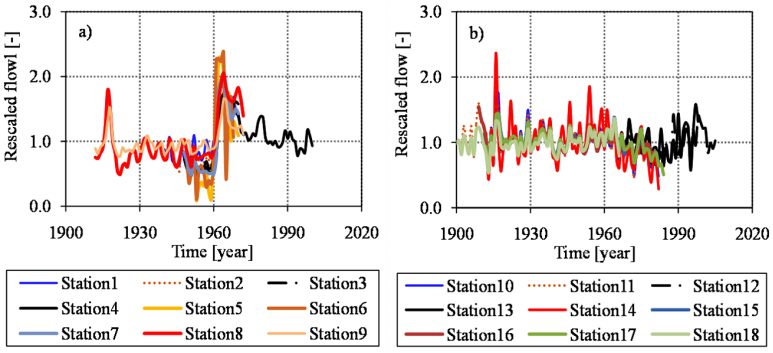

Figure 3. Variation in the annual flow of **(a)** group 1, and **(b)** group 2.

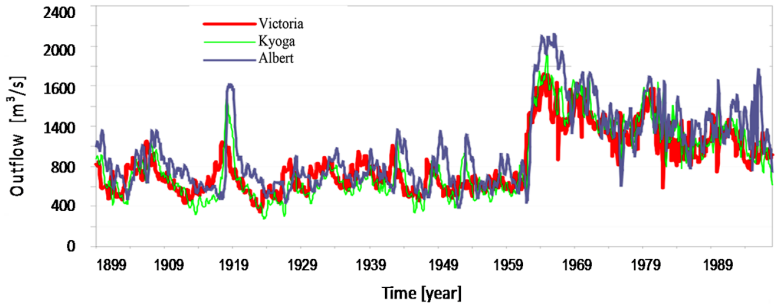

Figure 4. Variation in the annual outflows from the Lake Victoria, Kyoga and Albert over the period 1899 to 1997 (adopted from MWLE, 2004).

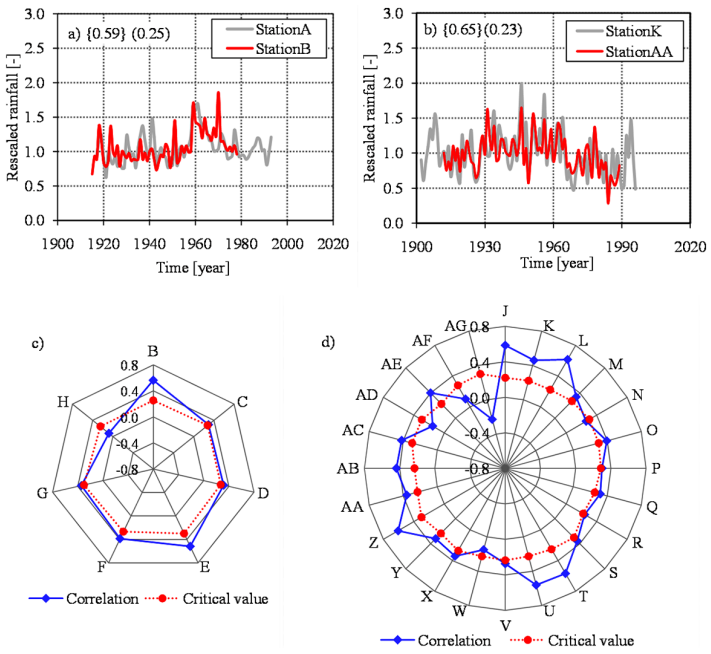

Figure 5. Variation in the annual rainfall at selected stations in **(a)** group 1, **(b)** group 2. Correlation between annual rainfall over **(c)** group 1 region and that at station A, **(d)** group 2 region and that at station I. In charts **(a, b)**, the labels { } and ( ) denote the correlation and its critical value. The critical values in all the charts are at significance level of 5 %. The letters B to AA denote the IDs for the rainfall stations as in Table 3.

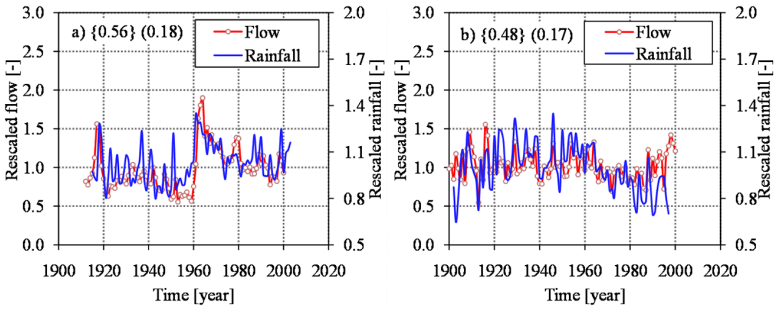

Figure 6. Variation in the region-wide annual flow and rainfall for **(a)** group 1, **(b)** group 2. The label in { } show the correlation between the annual rainfall and flow variation; and ( ) comprises the correlation critical values at 5 % significance level.

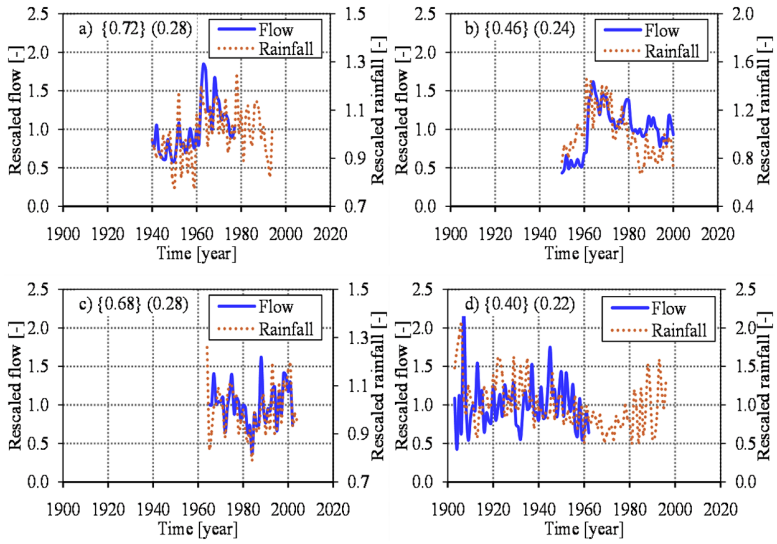

Figure 7. Variation in the annual flow and catchment-wide rainfall in **(a)** Kagera, **(b)** Kyoga, **(c)** Blue Nile, and **(d)** Atbara. The label in { } shows the correlation between the rainfall and flow; and ( ) comprises the correlation critical values at 5 % significance level.

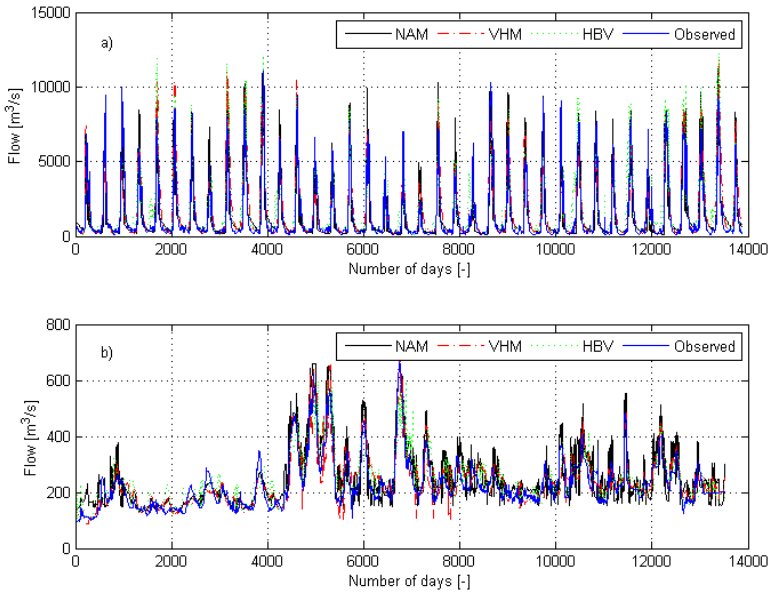

Figure 8. Simulated vs. observed daily flow for **(a)** Blue Nile, and **(b)** Kagera catchments. The calibration (validation) period cover the days 1–9131 (9132–13 879) for Blue Nile, and 1–9131 (9132–13 514) for Kagera.

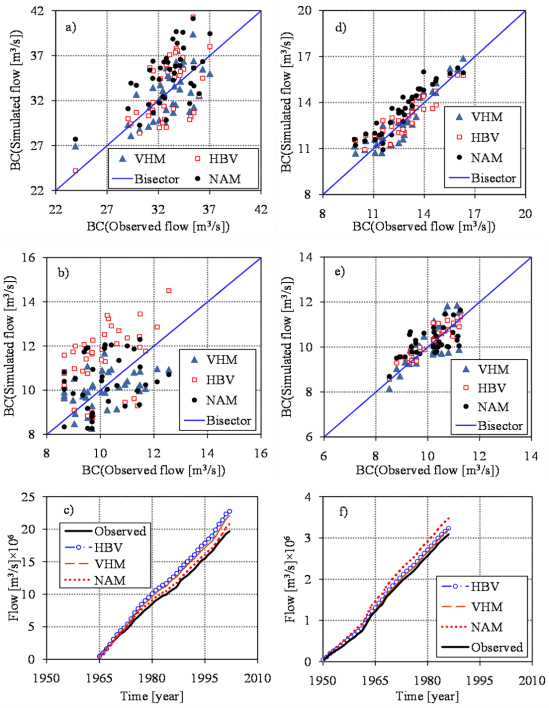

Figure 9. Evaluation of the model performance considering Box–Cox (BC) transformed **(a, d)** maximum flow in a year, **(b, e)** minimum flow in a year. Charts **(c, f)** are for cumulative flow, **(a–c)** Blue Nile catchment and **(d–f)** Kagera catchment.

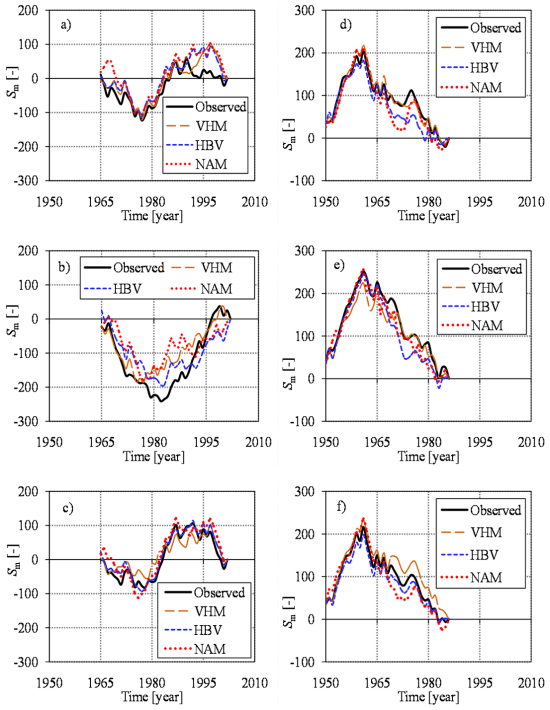

Figure 10. Comparison between observed and modeled overland flow in terms of the CRD plots for **(a)** annual maxima, **(b)** annual minima and **(c)** annual mean. The charts **(a–c)** and **(e, f)** are for the Blue Nile and Kagera catchments respectively.

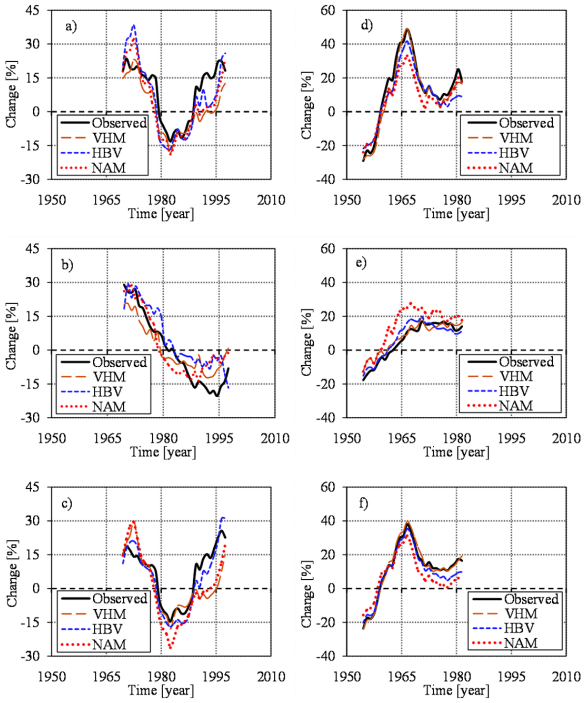

Figure 11. QPM results for observed and modeled overland flow in terms of anomalies in the **(a)** annual maxima, **(b)** annual minima and **(c)** annual mean. The charts **(a–c)** and **(e, f)** are for Blue Nile and Kagera catchments respectively.